

# Finite Difference Time Domain Modeling of Steady State Scattering from Jet Engines with Moving Turbine Blades

PROGRESS REPORT

Covering the period of  
September 25, 1991 to March 25, 1992

for

Grant NAG-1-1350

submitted to

Mr. Fred Beck

GCD, M/S 490  
National Aeronautics and Space Administration  
Langley Research Center  
Hampton, VA 23665-5225

and to

Captain Doug Havens  
AFEWC/ESAS  
San Antonio, TX 78243-5000

submitted by

Deirdre A. Ryan, H. Scott Langdon,  
John H. Beggs, David J. Steich,  
Raymond J. Luebbers and Karl S. Kunz

The Pennsylvania State University  
Department of Electrical and Computer Engineering  
University Park, PA 16802

submitted on

May 4, 1992

N92-30753

Uncles

03/07 0096921

(NASA-CR-190290) FINITE DIFFERENCE  
TIME DOMAIN MODELING OF STEADY  
STATE SCATTERING FROM JET ENGINES  
WITH MOVING TURBINE BLADES. PROGRESS  
REPORT, 25 SEP. 1991 - 25 MAR. 1992  
(Pennsylvania State Univ.) 35 p

## TABLE OF CONTENTS

I. Purpose . . . . .	3
II. Introduction . . . . .	3
III. Engine Geometry . . . . .	4
IV. Problem Space Termination . . . . .	7
V. Moving Objects . . . . .	9
A. Single Grid Approaches . . . . .	9
B. Dual Grid Approach . . . . .	10
VI. Summary . . . . .	14
VII. References . . . . .	15
VIII. Figure Titles . . . . .	17

## I. Purpose

The purpose of this progress report is to summarize the research progress for grant NAG-1-1350 entitled "Finite Difference Time Domain Modeling of Steady State Scattering from Jet Engines with Moving Turbine Blades" for the time period 9/25/91-3/25/92.

## II. Introduction

Steady state scattering, especially determination of Radar Cross Section, from jet engines with moving turbine blades is a difficult problem. Doppler frequency components are to be expected in the frequency domain scattering response and could be used to detect the rotational speed of the engine and hence possibly the type of engine. This is of great significance to detection and target identification for current and future defense/navigational radar systems.

The approach chosen to model steady state scattering from jet engines with moving turbine blades is based upon the Finite Difference Time Domain (FDTD) method. The FDTD method is a numerical electromagnetic program based upon the direct solution in the time domain of Maxwell's time dependent curl equations throughout a volume. One of the strengths of this method is the ability to model objects with complicated shape and/or material composition. General time domain functions may be used as source excitations. For example: a plane wave excitation may be specified as a pulse containing many frequencies and at any incidence angle to the scatterer. A best fit to the scatterer is accomplished using cubical cells in the standard cartesian implementation of the FDTD method. The material composition of the scatterer is determined by specifying its electrical properties at each cell on the scatterer. Thus, the FDTD method is a suitable choice for problems with complex geometries evaluated at multiple frequencies. It is assumed that the reader is familiar with the FDTD method. References [1]-[3] provide general background information on the method.

The challenges are many in this analysis. Upon first glance the most difficult task appears to be the integration of moving objects into a stationary analysis. However, other factors must also be considered. Namely, the jet engine appears to be a resonant cavity with a high  $Q$ . This means that the electromagnetic energy that penetrates the inlet stays inside for a very long time. This in turn requires a much longer computation time in order to reach the steady state field value. Another obstacle must be overcome in addition to the two impediments mentioned already: the size of the scatterer. The

issue here is not with the volume the scatterer occupies within the problem space but with the shape and the dissimilar proportions of the components of the scatterer. These three issues are discussed in the following sections.

### III. Engine Geometry

A brief review of the FDTD method has already been conducted. This section is concerned with the scattering object that is constructed in the problem space. The scatterer is located in the volume by discretizing the object into cubical cells and assigning electrical characteristics (permittivity, conductivity) to each individual cell in the x, y, and z directions. The scatterer is easily modified simply by changing the electrical characteristics at individual cell locations. The ability to change the scattering object (the volume) is one of the strengths of the FDTD method.

One of the difficulties inherent to FDTD is the problem space size. The issue here is twofold. The scatterer is large and the actual volume the scatterer occupies within the problem space is appreciable. Additionally, the shape and dissimilar proportions of the components of the scatterer are of concern. And still other issues must be considered based on the characteristics of scatterer, both electrical and geometrical.

First let us examine the size of the problem space. In order to size the problem one must consider the machine on which the problem may be evaluated. The computer on which this calculation is based is a Silicon Graphics workstation with 64 MB of RAM. The standard Yee unit cell (Figure 1) is used and requires six real field component variables as well as three integer\*1 material property variables for characterization of perfect electrical conductor, dielectric and lossy dielectric structures. This yields a total of nine variables per cell. Each field variable requires 4 bytes of memory and each material property variable requires 1 byte of memory so 27 bytes are required to store variables for each cell. The limit of RAM accessible for a computation on this workstation is approximately 60 MB since 4 MB must be reserved for system utilization.

In order to maximize utilization of the problem space volume the geometry of the scatterer must be considered. Since aircraft engines are longer than they are wide, the engine inlet is chosen to be four times as long as it is wide, Figure 2. The cell volume of the scatterer may be expressed as  $x$  by  $x$  by  $4x$  which equals  $4x^3$ . The variable  $x$  represents the total number of cells across the short dimension. Now let us determine the number of cells along the short dimension of the problem space  $x$ :

$$\text{Volume} = \frac{\text{Available RAM}}{\text{storage per cell}}$$

$$4x^3 = \frac{60 * 2^{20} \text{ bytes}}{27 \text{ bytes}}$$

$$4x^3 = 2.33 * 10^6$$

$$\Rightarrow x = 83.5 \text{ cells .}$$

Assuming that a 10 cell border must surround the scattering object, the available cells for modeling are  $73 \times 73 \times 292 = 1,556,068$ . For a small engine with a diameter of 1.0 m the cell size  $\Delta x$  is

$$\Delta x = \frac{\text{Engine diameter}}{\text{modeling cells}}$$

$$\Delta x = \frac{1.0 \text{ m}}{73 \text{ cells}}$$

$$\Rightarrow \Delta x = 1.37 \text{ cm.}$$

With  $\Delta x = 1.37$  cm and a resolution of 10 cells per wavelength the maximum frequency allowable is 2.19 GHz.

Not only is the scatterer very large, but it also contains fine components, see Figure 3. The moving parts of the engine are of interest in this analysis and the smallest components, such as the hoses and wires, will not be considered at this time. The dilemma is to accurately render the turbine blades when restricted to a minimum cell size by the computational machine limits.

Other difficulties occur when the geometrical configuration of the scatterer is a semi-closed shape. Contrary to intuition, electromagnetic energy penetrates a semi-closed structure and, depending on the loss characteristics of the material, remains inside for long periods of time. Once the energy is inside of the semi-closed structure the frequencies of the penetrating signal are re-tuned to the resonant frequencies of the structure [4]. Thus the semi-closed structure is resonant at certain frequencies dictated by the geometrical configuration of the structure. The quality factor,  $Q$ , relays the resonant information of a structure. High  $Q$  values indicate extremely resonant cavities. The high  $Q$  of the engine means that the computation must be run for a greater number of time steps if the conventional post-processing approach is used on the time domain results.

The FDTD method has been applied to resonant cavities [5]. Based on this analysis and the geometrical configuration and electrical properties of the engine, it is likely that the engine is a highly resonant structure. The engine appears to be a semi-closed structure due to the overlapping blades of the compressor at the front and the turbine at the back of the engine. This combined with the low loss material (metal) of the engine components cause the scatterer to be a resonant structure. Therefore electromagnetic energy within the scatterer lingers for a long time. Hence, a significant number of time steps will be required. Using the  $\Delta x$  of 1.37 cm calculated previously the time step  $\Delta t$  is

$$\Delta t = \frac{\Delta x}{\sqrt{3} c}$$

$$\Delta t = \frac{1.37 \text{ cm}}{\sqrt{3} (3.0 * 10^8 \text{ m/s})}$$

$$\Rightarrow \Delta t = 26.4 \text{ ps.}$$

Estimating that most of the energy has dissipated by 1  $\mu$ s, the number of time steps required is

$$TIME \ STEPS = \frac{Cavity \ decay \ time}{\Delta t}$$

$$TIME \ STEPS = \frac{1.0 * 10^{-6}}{26.4 * 10^{-12}}$$

$$\Rightarrow TIME \ STEPS = 37,928.$$

The cavity decay time may be smaller than this when the effects of loss in the engine, e.g. carbon from burning fuel, are included.

Having discussed the size of the scatterer and its predisposition to retain energy, a first attempt at depicting the engine geometry is shown in Figure 4. Figures 5, 6 and 7 show the front view, side view and the centerline slice of the engine. This is a zeroth order model and serves as a good starting point for determining the resonance of the engine and the effectiveness of the Motion FDTD computation in evaluating the rotating parts of the engine. The zeroth order model has been verified using a three dimensional FORTRAN graphics program on the Silicon Graphics workstation.

The zeroth order model is constructed in three main parts. The outside of the engine is called the inlet and is circular cylindrical in shape and hollow inside. The inlet is the

stationary part of the engine. The moving components are the rotor shaft and the blades. The shaft is modeled as a solid circular cylinder which extends from the front to the rear of the inlet. The blades form a planar fan in the zeroth order model. The fans are identical and one represents the compressor at the front of the engine and the other represents the turbine at the rear. The two-dimensional fans lie in the plane normal to the engine axis and intersect the axis at the front and rear of the inlet. The zeroth order model is automated and the user specifies the number of blades in the fan unit, the thickness of the blades, the radius of the rotor shaft, the radius of the blades, and the radius of the engine inlet.

The number of blades specified for this model must be even. The blades are distributed symmetrically about the engine axis. The base of the blade starts on the shaft at  $r_{\text{SHAFT}}$  and the tip of the blade extends to  $r_{\text{BLADE}}$ . The width of the blade refers to the area between the two radii that may be metal. The width of the blade controls the openness of the engine. By specifying the number of blades and the width of metal to air of the blade arc, the model serves to approximate the overlapping blades of a turbine/compressor assembly. In this way the ratio of air to metal in the planar fan remains constant but the occurrence of the air to metal pattern increases and the arc length subtended by each decreases as the number of blades increases.

The number of blades, NB, is specified and a new blade starts every  $\theta_{\text{incr}}$  where incr stands for increments and

$$\theta_{\text{incr}} = \frac{2\pi}{\text{NB}} .$$

The ratio of metal to air, BLDWD, is specified as a real number between 0.0 and 1.0. If a zero is specified the fan structure is not constructed, i.e. the blades have zero thickness so the fan is air. When a one is specified the fan structure becomes an solid metal disk (like a coin), i.e. the blades completely fill the planar fan with metal. If 0.5 is specified this means that half of the blade is metal and half is air. Thus for the first blade the metal starts at 0.0 degrees and continues until  $\Delta\theta$  where

$$\Delta\theta = \text{BLDWD} * \theta_{\text{incr}} .$$

The remainder of the angle from  $\Delta\theta$  to  $\theta_{\text{incr}}$  is air. Figure 8 illustrates these variables for one blade of the planar fan. Figure 5 depicts the blade structure when eight blades are specified and BLDWD is 2/3.

Using the zeroth order model of the engine, we plan to investigate the Q of the cavity. The next model of the engine

will be based on the zeroth order model. The rotor and inlet will be the same and the fan will be extended to three dimensions. The decay rates of the fields in the zeroth order and first order model will be compared. This will be useful in determining whether a three dimensional Motion FDTD algorithm is in order or if a two dimensional Motion FDTD algorithm may be used. Note that if the fields in both models behave similarly then the zeroth order model of the turbine/compressor assembly might suffice. However if the scatter from the first order model using a three dimensional fan is markedly different from the scatter from the zeroth order model, the next order model might have to be used. The effect of the three dimensional fan on the cavity fields of the engine will be investigated in the next time period.

#### IV. Problem Space Termination

It is evident from the discussion above that any computational savings is welcome. With this in mind, consider that additional cells must be added to the exterior of any scattering object evaluated using FDTD in order to lower the erroneous reflection from the problem space termination. At the very least a ten cell free space border must be attached to every dimension of the scatter when applying the second order absorbing boundary conditions developed by Mur [6]. However, when the scattered fields are highly reactive or when the scattered fields are not normally incident to the absorbing cells, even a ten cell border does not prevent large reflections from the problem space termination.

An improvement to the absorbing boundary conditions developed by Mur has been tested. The improved boundary conditions are called Super Outer Radiating Boundary Conditions, Super ORBC, or SORBC [7]. The SORBC minimize the non-normal incidence and reactive errors mentioned above.

Determination of the electric and magnetic field at the termination of the computational grid using the SORBC involves several steps. First, the incidence angle of the scattered field at each border cell is determined from the Poynting vector. Next, electric and magnetic fields are estimated as follows. The first order Mur equations are used to predict edge electric field components from the inner electric field components. The same equations are then used to predict an edge magnetic field component. The estimated magnetic field component is used by the finite difference equations to estimate yet another electric field value. This results in two different estimates of the electric field for each border cell. Finally, both estimated electric field values are utilized using a weighted average. The



two estimated electric fields are added using a weighted average which depends on the arrival angle of the Poynting vector.

The SORBC provides more accurate results than the second order Mur equations because the incidence angle is included in the calculation. The SORBC have been verified and will be described in more detail in the next progress report.

## V. Moving Objects

One of the difficulties in this problem is because of the moving objects that are present in the analysis. An approach needs to be developed that properly treats the physical phenomena involved with scattering from moving objects and this approach needs to be adaptable to the FDTD method. Another difficulty arises in incorporating any approach into the FDTD method because of the moving objects. In the FDTD method, the object and surrounding computational space are sampled at discrete points in space and electric and magnetic fields are interleaved on this spatial grid. Once an object begins to move, it is no longer "attached" to the grid and becomes more difficult to analyze using FDTD. A discussion of the two main approaches investigated follows.

### A. Single Grid Approaches

The first approach tried for simulating moving objects in FDTD was to allow the object to move one cell every  $N$  time steps.  $N$  is calculated from the duration of one time step to give the desired speed: eg.  $N = (\Delta x/v_x)/\Delta t$ , where  $v_x$  is the x-component of velocity. This is referred to as the "jumping-cell" algorithm because the moving object appears to suddenly pass or "jump" from one cell to the next every  $N$  time steps. The fields and constitutive parameters associated with a moving cell are copied to the new location so there is a crude approximation of charge flow along with motion of the object boundary. In spite of approximating the charge flow at the object boundary, this technique is still very non-physical. One reason is the relatively large discontinuity that occurs between the two adjacent time steps every time the object moves. Another reason is the failure to model the instantaneous field changes in front of the object. Figure 9 shows the results of this simulation on the E-field backscattered from a perfectly conducting slab. In this figure, the scattered field from a stationary slab is compared with that from the same object in "motion." The slab velocity in the moving case is  $c/100$  m/s, which should give a frequency shift of about 10 MHz. No shift is noticed, though sidebands are produced at harmonics of the cell moving rate.

The second approach, referred to here as the "growing-cell" algorithm, is a significant refinement of the above procedure. The "growing-cell" approach allows the object to move a fraction of a cell length every time step. Consider the free space cell directly in front of a moving conductor, where the conductor velocity is normal to its surface. This is shown in Figure 10. The integral form of Maxwell's electric curl equation expressed around the perimeter of this cell is

$$\oint \bar{E} \cdot d\bar{s} = -\left(\frac{\partial}{\partial t}\right) \iint \bar{B} \cdot d\bar{S} = -\iint \frac{\partial \bar{B}}{\partial t} \cdot d\bar{S} + \int_0^1 \bar{B} \cdot (\bar{v} \times d\bar{l}) \quad .$$

In finite difference form this gives (for velocity in the x-direction)

$$H_x^{n+1/2} = H_x^{n-1/2} + \frac{\Delta t}{\mu} \left( \frac{\Delta E_y}{\Delta z} - \frac{\Delta E_z}{\Delta y} \right) + \frac{v_x}{\sqrt{3} c} H_x^{n-1/2}$$

$$H_y^{n+1/2} = H_y^{n-1/2} + \frac{\Delta t}{\mu} \left( \frac{\Delta E_z}{\Delta x} - \frac{\Delta E_x}{\Delta z} \right) + \frac{v_x}{\sqrt{3} c} H_y^{n-1/2} \quad .$$

Results for this approach are given in Figure 11 for the same problem geometry and slab velocity as in Figure 9. The moving slab case shows the correct Doppler frequency shift, although sidebands are still produced and the Doppler amplitude, which should have increased less than a dB, is incorrect.

### B. Dual Grid Approach

The Dual Grid approach involves a Lorentz type of transformation of the field components and interpolation into the FDTD grid.

A recent paper [8] describes electromagnetic scattering from moving surfaces in one and two dimensions using the FDTD method. In that paper, the motion of the surfaces were tracked in the FDTD code and the relativistic boundary conditions were implemented at each surface and the total fields were set to 0 inside each conductor. The results in the paper agreed reasonably well with published results, but the limitations are that only perfect conductors were considered and the analysis was not generalized. The paper also mentions the approach of using a Lorentz transformation of the incident field to the moving system and then solving the scattering problem in the moving system where the geometry is stationary. The final step involves a Lorentz transformation back to the inertial frame of reference. This is the basic approach that is developed for the present work.

Since jet engine turbine blades exhibit strictly rotational motion, our approach is based upon a transformation to and from a rotating system of coordinates. Many articles have been published regarding Maxwell's equations in rotating systems and the solution of scattering problems with rotating objects [9]-[19]. Maxwell's equations are invariant under any coordinate transformation, but the constitutive equations are modified. Let us denote the laboratory frame of reference as F, the rotating frame of reference R and quantities in frame F will be unprimed and those in frame R will be primed. The rotating frame R has a constant angular velocity  $\Omega$  (see Figure 12). In the laboratory frame, Maxwell's curl equations are [16]

$$\begin{aligned}\bar{\nabla} \times \bar{E} &= -\frac{\partial \bar{B}}{\partial t} \\ \bar{\nabla} \times \bar{H} &= \frac{\partial \bar{D}}{\partial t} + \bar{J}\end{aligned}\quad (1)$$

and the constitutive relations become modified as

$$\begin{aligned}\bar{B} &= \mu [\bar{H} - \bar{v} \times \bar{D}] + \frac{1}{c^2} \bar{v} \times \bar{E} \\ \bar{D} &= \epsilon [\bar{E} + \bar{v} \times \bar{B}] - \frac{1}{c^2} \bar{v} \times \bar{H} \\ \bar{J} &= \gamma \sigma \left[ \bar{E} + \bar{v} \times \bar{B} - \frac{\bar{v}}{c} \left( \frac{\bar{v}}{c} \cdot \bar{E} \right) \right] + \rho \bar{v}\end{aligned}\quad (2)$$

where

$$\bar{v} = \bar{\Omega} \times \bar{r}, \quad \gamma = \frac{1}{\sqrt{1-\beta^2}}, \quad \beta = \frac{v}{c}\quad (3)$$

$c$  is the speed of light in free space and  $\rho$  is charge density.

The transformation to rotating coordinates is given by

$$\begin{aligned}x' &= x \cos(\Omega t) + y \sin(\Omega t) \\ y' &= -x \sin(\Omega t) + y \cos(\Omega t) \\ z' &= z \\ t' &= t \\ \phi' &= \phi - \Omega t\end{aligned}\quad (4)$$

and the inverse transformation is obtained from (4) by interchanging the primed and unprimed variables and replacing  $\Omega$  by  $-\Omega$ . Maxwell's curl equations remain invariant in rotating coordinates and are given by

$$\begin{aligned}\bar{\nabla}' \times \bar{E}' &= -\frac{\partial \bar{B}'}{\partial t'} \\ \bar{\nabla}' \times \bar{H}' &= \frac{\partial \bar{D}'}{\partial t'} + \bar{J}'\end{aligned}\quad (5)$$

with the constitutive relations defined by

$$\begin{aligned}\bar{B}' &= \mu \bar{H}' + \frac{1}{c^2} \bar{v} \times \bar{E}' \\ \bar{D}' &= \epsilon \bar{E}' - \frac{1}{c^2} \bar{v} \times \bar{H}' \\ \bar{J}' &= \sigma \bar{E}' .\end{aligned}\quad (6)$$

The transformation of the field components is given by

$$\begin{aligned}\bar{E}' &= \bar{E} + \bar{v} \times \bar{B} \\ \bar{H}' &= \bar{H} - \bar{v} \times \bar{D} \\ \bar{B}' &= \bar{B} \\ \bar{D}' &= \bar{D} .\end{aligned}\quad (7)$$

In this approach, two FDTD grids are used in the analysis. One grid is a stationary grid and is located in the laboratory (or inertial reference) frame and the other is a grid that is "attached" to the rotating object (see Figure 13). The stationary grid will be a minimum of  $\sqrt{2}$  cells larger on a side than the rotating grid so that all field components contained in the rotating grid will remain inside the stationary grid as the blades rotate. Thus, the object remains stationary with respect to R, and the FDTD grid points are well defined within the rotating frame. However, as the object rotates, the grid points in R will no longer coincide with the grid points in the laboratory frame F. The procedure to obtain the FDTD field components in frame F will involve interpolation of the field components in frame R and then a transformation back to frame F. The full procedure is outlined as follows:

- 1.) Transform the incident field to rotating coordinates using (4).
- 2.) Compute field values in the rotating frame using (5) and (6).
- 3.) Apply boundary conditions in the rotating space R.
- 4.) Interpolate fields from the rotated space R spatial locations in R corresponding to FDTD field locations in the laboratory frame F.
- 5.) Transform interpolated fields from step 4 to the laboratory frame I using (7).
- 6.) Apply stationary FDTD equations to field components in the

laboratory frame F that were not interpolated from the rotating space R.

7.) Apply boundary conditions to the stationary grid.

Step 1 of this procedure has been successfully demonstrated using a two dimensional TM code containing only the FDTD incident field. Two grids were defined in the normal FDTD manner and the incident field was analytically specified as

$$E_z^i(t) = r(t) \sin(\omega_0 t)$$

where  $r(t)$  is a ramping function that transitions from 0 to 1 over several cycles of the sinusoid. For a test problem a sinusoidal frequency of 20 Hz was chosen so that Doppler frequency components would be very apparent. Of course, higher frequency incident fields and wideband pulses will be used in the full analysis. A point within the FDTD grid was chosen and the incident field was computed both in the stationary grid and the rotating grid. For  $\Omega=0$ , both incident fields were identical as expected. According to [17], the incident field in rotating coordinates should exhibit an infinite number of sidebands corresponding to

$$\omega_m = \omega_0 + m\Omega \quad (8)$$

for nonvanishing  $\Omega$ . This behavior does not become readily apparent in the frequency response until  $\Omega$  becomes on the order of  $\omega_0$ . Figures 14-15 show the time and frequency domain response of the incident field in stationary and rotating coordinates for  $\Omega=2\pi$  rad/sec corresponding to  $\Omega/\omega_0=0.05$ . Note that the time domain rotating incident field is almost identical to the stationary incident field except for a slight time shift (corresponding to a phase shift). The frequency response of the rotating incident field is slightly shifted from the stationary response due to the smearing of the sideband components that are spaced only 1 Hz apart. Figures 16-17 show the time and frequency domain incident field for  $\Omega=20\pi$  rad/sec corresponding to  $\Omega/\omega_0=0.5$ . Note that the rotating time domain field is now markedly different than the stationary field and Figure 17 shows the frequency response indicating the sidebands spaced 10 Hz apart according to (8). These effects were also seen for larger ratios of  $\Omega/\omega_0$ .

The dual grid approach shows the most promise at this point for a computational approach to modelling rotating objects. The incident field in the rotating system exhibits sidebands at multiples of the rotational speed according to theory. The next phase of development is to test this approach on a two-dimensional problem similar to one analyzed in [19] and compare with another computational or analytic solution. If the approach works on a two-dimensional test problem, then it can be generalized to three dimensions to analyze an engine geometry

complete with canted rotor and turbine blades. An improvement to the brute-force dual grid approach which will also be investigated is to apply the dual grid technique on a local basis for only those portions of the engine that are rotating. This improvement would make the dual grid approach more efficient since two three-dimensional grids would not be used thereby decreasing memory and CPU requirements.

## VI. Summary

Referring to the Statement of Work for "Finite Difference Time Domain Modeling of Steady State Scattering from Jet Engines with Moving Turbine Blades," many of the preliminary tasks have been completed or are near completion. The status of and a brief summary of the tasks attempted during this time period follow.

### Task 1: Automate Target Geometry Input

An automated engine geometry computer code was developed. This model is called the zeroth order model because the turbine/compressor fan is confined to a plane. The user initializes several engine dimensions and the material properties at each FDTD cell are automatically assigned.

### Task 2: Graphical Verification of Target Geometry

The graphical verification of the engine geometry was developed in conjunction with the zeroth order engine model. A three dimensional graphics program for visualization of the three dimensional engine geometry was completed. This program is written in FORTRAN and utilizes the graphics library on a Silicon Graphics workstation.

### Task 3: Graphical Display of Electromagnetic Fields

A program to show the electromagnetic fields in the problem space is near completion.

The absorbing boundary conditions at the edge of the computational grid have been improved. The modified grid termination equations, the SORBC, reduce reflection errors attributed to non-normal incidence angles and highly reactive fields.

Several approaches to modeling the rotating objects in the jet engine using FDTD were considered. Further investigation of both the Single Grid Approach and the Dual Grid Approach is needed.

## VII. References

- [1] K. S. Yee, "Numerical Solution of Initial Boundary Value Problems Involving Maxwell's Equations in Isotropic Media," IEEE Trans. on Antennas and Propagat., pp. 302-307, May 1966.
- [2] A. Taflove and K. Umashankar, "Finite-Difference Time-Domain (FD-TD) Modeling of Electromagnetic Wave Scattering and Interaction Problems," IEEE Antennas and Propagat. Soc. Newsletter, pp. 5-20, Apr. 1988.
- [3] A. Taflove, "Review of the formulation and applications of the finite-difference time-domain method for numerical modeling of electromagnetic wave interactions with arbitrary structures," Wave Motion, vol. 10, Dec. 1988.
- [4] K. S. Kunz, private communication.
- [5] K. S. Kunz, D. J. Steich and R. J. Luebbers, "Low Frequency Shielding Effects of a Conducting Shell with an Aperture: Response of an Internal Wire," IEEE Trans. Electromagn. Compat., accepted for publication.
- [6] G. Mur, "Absorbing boundary conditions for finite-difference approximation of the time-domain electromagnetic-field equation," IEEE Trans. Electromagn. Compat., vol. EMC-23, pp. 1073-1077, Nov. 1981.
- [7] J. Fang and K. K. Mei, "A super-absorbing boundary algorithm for solving electromagnetic problems by time-domain finite-difference method," in Proc. 1988 IEEE AP-S Int. Symp. (Syracuse, NY), June 1988, pp. 472-475.
- [8] F. Harfoush, A. Taflove, and G. A. Kriegsmann, "A numerical technique for analyzing electromagnetic wave scattering from moving surfaces in one and two dimensions," IEEE Trans. on Antennas and Propagat., vol. 37, pp. 55-63, Jan. 1989.
- [9] L. I. Schiff, "A Question in General Relativity," Proc. Natl. Acad. Sci., vol. 25, pp. 391-395, 1939.
- [10] M. G. Trocheris, "Electrodynamics in a Rotating Frame of Reference," Phil. Mag., vol. 40, pp. 1143-1154, 1949.
- [11] J. Ise and J. L. Uretsky, "Vacuum Electrodynamics on a Merry-Go-Round," Amer. Journal Physics, vol. 26, pp. 431-435, Oct. 1958.
- [12] W. M. Irvine, "Electrodynamics in a Rotating System of Reference," Physica, vol. 30, pp. 1160-1170, 1964.

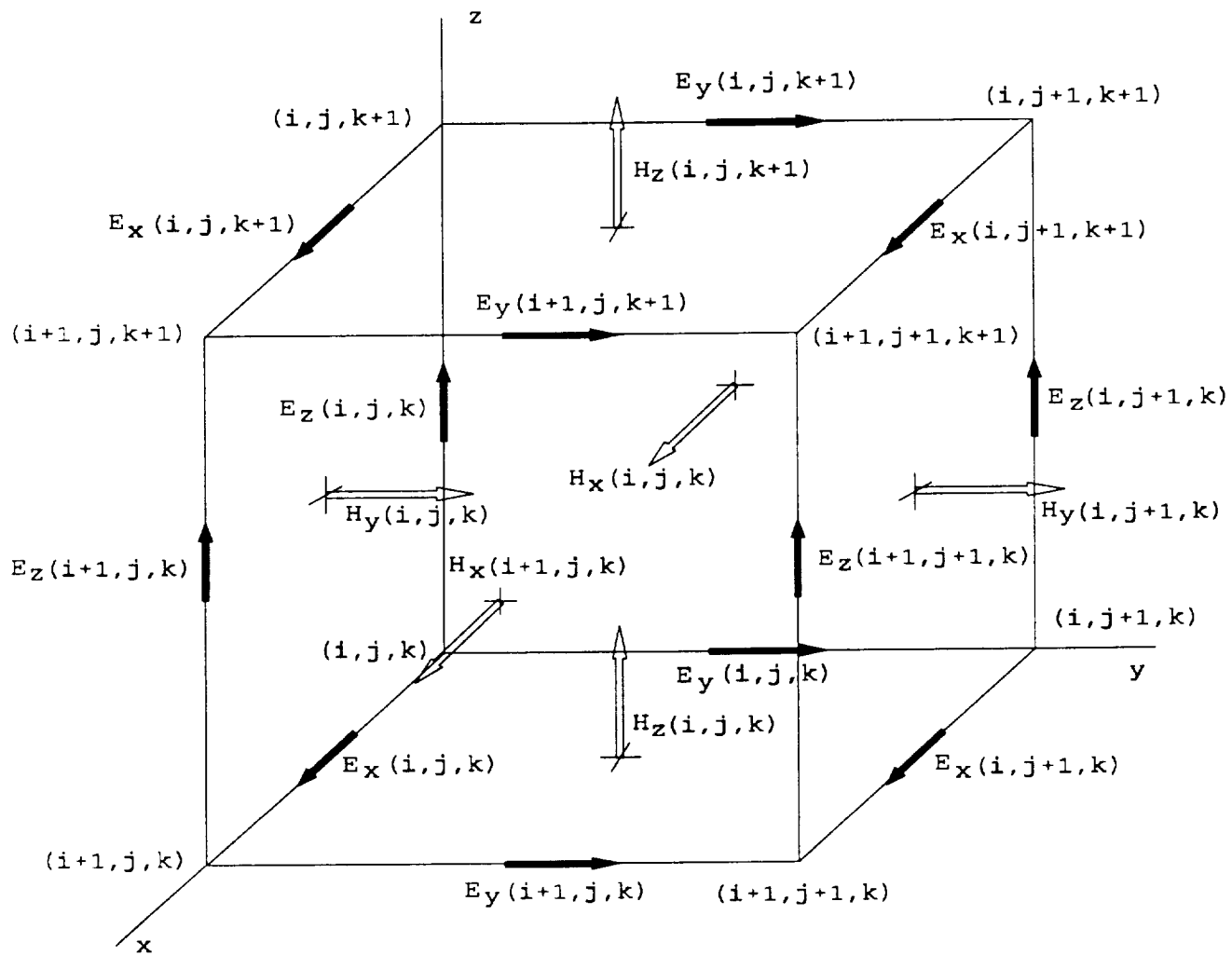
- [13] G. E. Modesitt, "Maxwell's Equations in a Rotating Reference Frame," Amer. Journal Physics, vol. 38, pp. 1487-1489, Dec. 1970.
- [14] J. Van Bladel, "Relativistic Theory of Rotating Disks," Proc. IEEE, vol. 61, pp. 260-268, March 1973.
- [15] D. L. Webster and R. C. Whitten, "Which Electromagnetic Equations Apply in Rotating Coordinates?," Astrophys. Space Sci., vol. 24, pp. 323-333, 1973.
- [16] T. Shiozawa, "Phenomenological and Electron-Theoretical Study of the Electrodynamics of Rotating Systems," Proc. IEEE, vol. 61, pp. 1694-1702, Dec. 1973.
- [17] J. Van Bladel, "Electromagnetic Fields in the Presence of Rotating Bodies," Proc. IEEE, vol. 64, pp. 301-318, March 1976.
- [18] H. Goto and T. Shiozawa, "Relativistic Solution to the Problem of Scattering by a Rotating Dielectric Column," J. Appl. Phys., vol. 49, pp. 556-561, Feb. 1978.
- [19] D. De Zutter, "Scattering by a Rotating Cylinder with Finite Conductivity," IEEE Trans. Antennas Propagat., vol. AP-31, pp. 166-169, Jan. 1983.



### VIII. Figure Titles

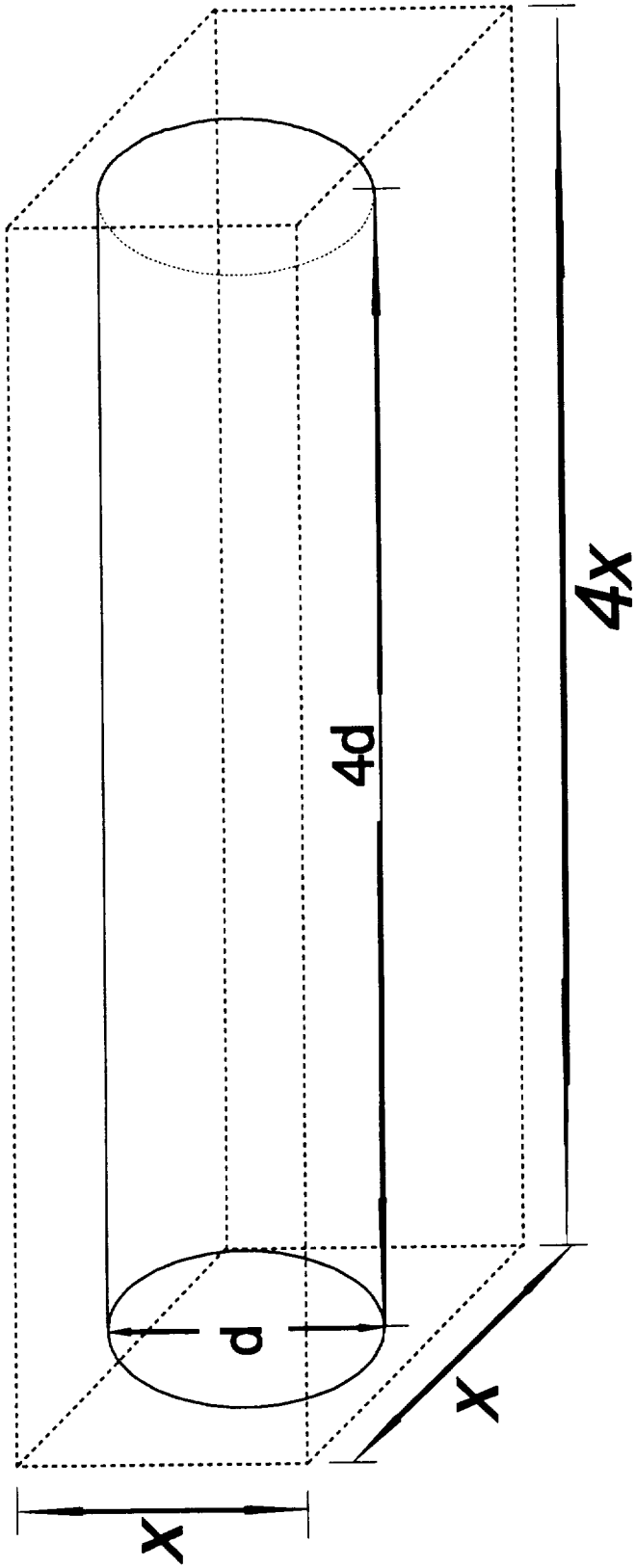
- 1.) Standard three-dimensional Yee cell showing placement of electric and magnetic fields.
- 2.) View of engine inlet showing diameter  $d$ , length  $4d$  and problem space dimensions  $x$  and  $4x$ .
- 3.) View of jet engine showing various components.
- 4.) View of jet engine inlet showing zeroth order geometry model.
- 5.) Front view of engine geometry for an eight blade example with variable  $BLDWD=2/3$  and showing various radii.
- 6.) Side view of engine geometry for the eight blade example of Figure 5.
- 7.) Centerline slice of engine geometry for the eight blade example of Figure 5.
- 8.) Zeroth order blade model showing variables  $\theta_{incr}$ ,  $\Delta\theta$ ,  $r_{shaft}$  and  $r_{blade}$ .
- 9.) Scattered electric field versus frequency for moving slab using "jumping-cell" algorithm with  $v=c/100$  m/s.
- 10.) Cell in free space immediately in front of moving conductor showing integration loop used to derive FDTD H-field update equation for "growing-cell" algorithm.
- 11.) Scattered electric field versus frequency for moving slab using "growing-cell" algorithm with  $v=c/100$  m/s.
- 12.) Inertial reference frame  $F$  and rotating frame  $R$ .  $R$  rotates with constant angular speed  $\Omega$  with respect to  $F$ .
- 13.) Two-dimensional stationary grid (unprimed quantities) and two-dimensional rotating grid (primed quantities) used for dual grid approach.
- 14.) Time domain incident field in stationary and rotating coordinates with  $\omega_0=40\pi$  rad/sec,  $\Omega=2\pi$  rad/sec and  $\Omega/\omega_0=0.05$ .
- 15.) Frequency response of incident field in stationary and rotating coordinates with  $\omega_0=40\pi$  rad/sec,  $\Omega=2\pi$  rad/sec and  $\Omega/\omega_0=0.05$ .
- 16.) Time domain incident field in stationary and rotating coordinates with  $\omega_0=40\pi$  rad/sec,  $\Omega=20\pi$  rad/sec and  $\Omega/\omega_0=0.5$ .

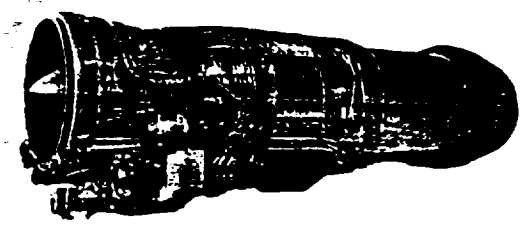
- 17.) Frequency response of incident field in stationary and rotating coordinates with  $\omega_0=40\pi$  rad/sec,  $\Omega=20\pi$  rad/sec and  $\Omega/\omega_0=0.05$ .



— Engine Inlet

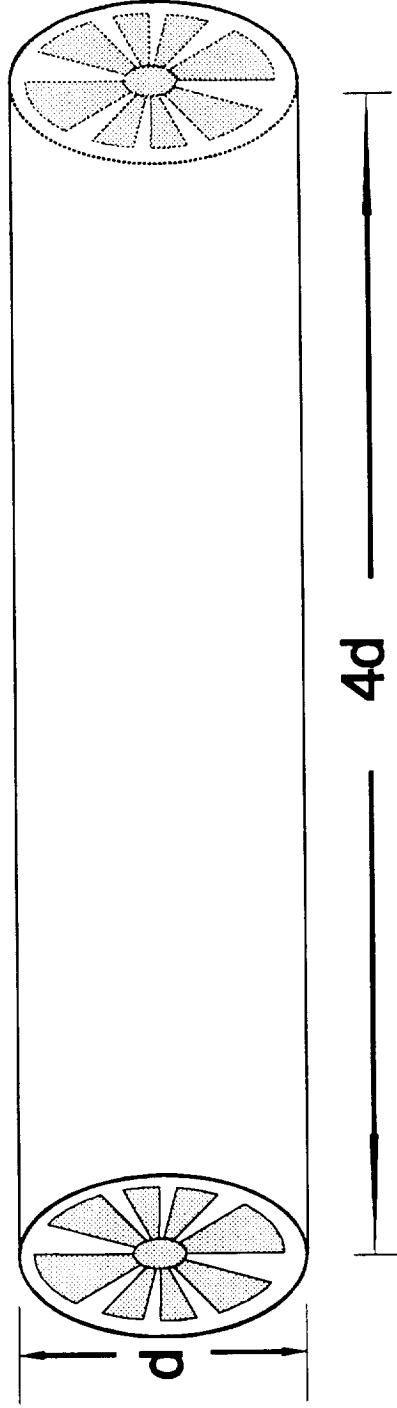
..... Problem Space



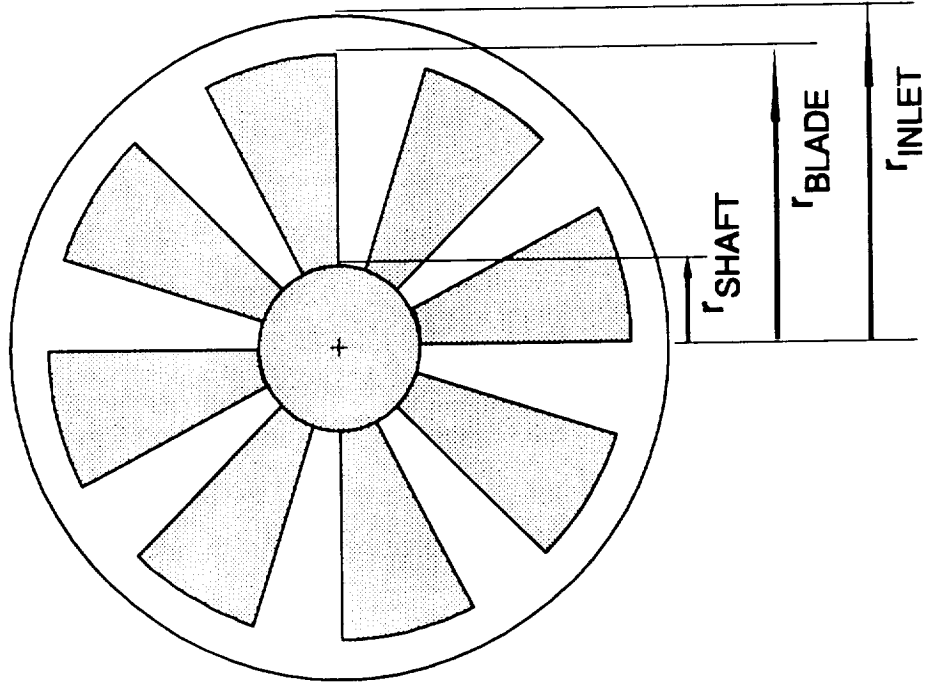


# Engine Inlet

## Zeroth Order Model



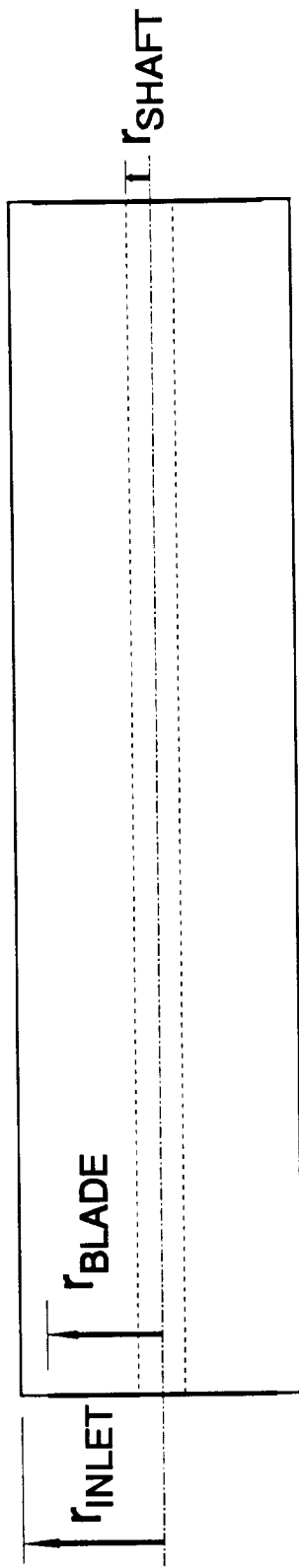
**Zeroth Order Engine Geometry**  
**8 Blade example**



**Front / Rear View**

# Zeroth Order Engine Geometry

## 8 Blade Example

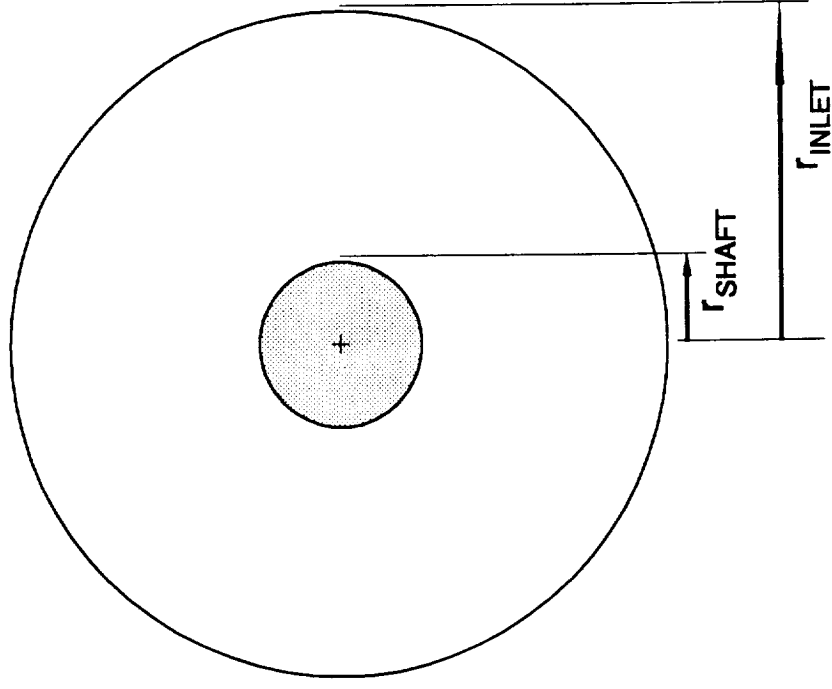


Side View



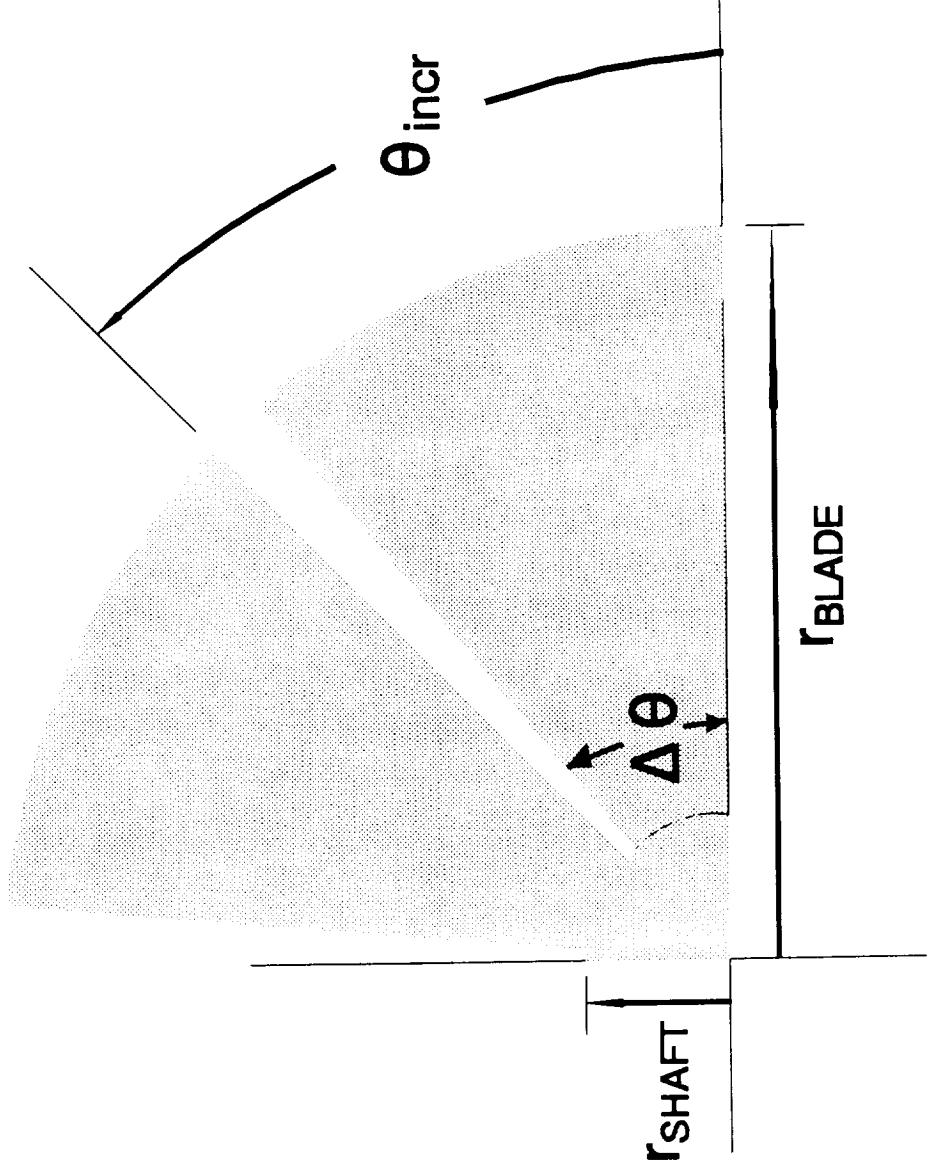
# Zeroth Order Engine Geometry

## 8 Blade example

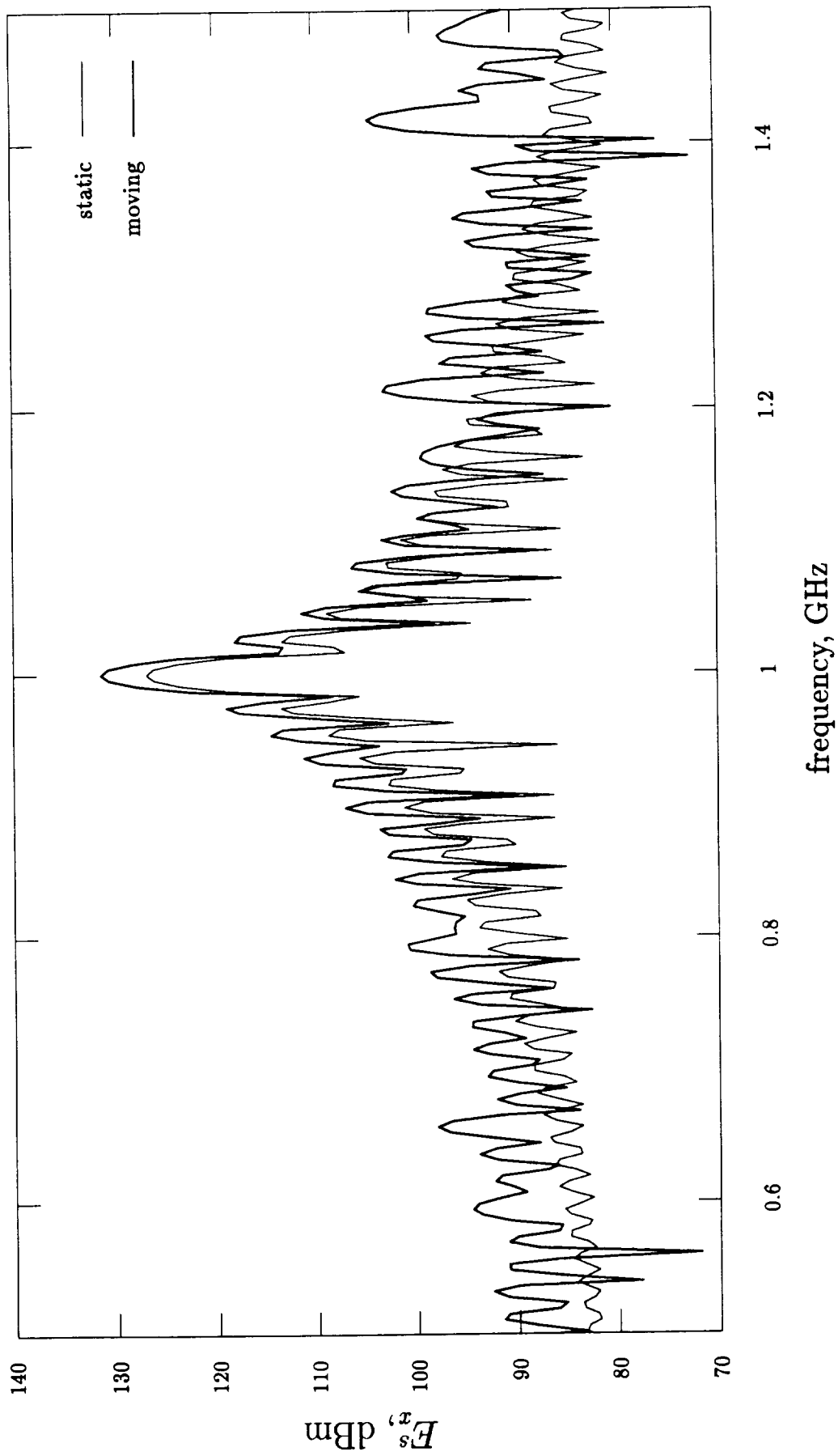


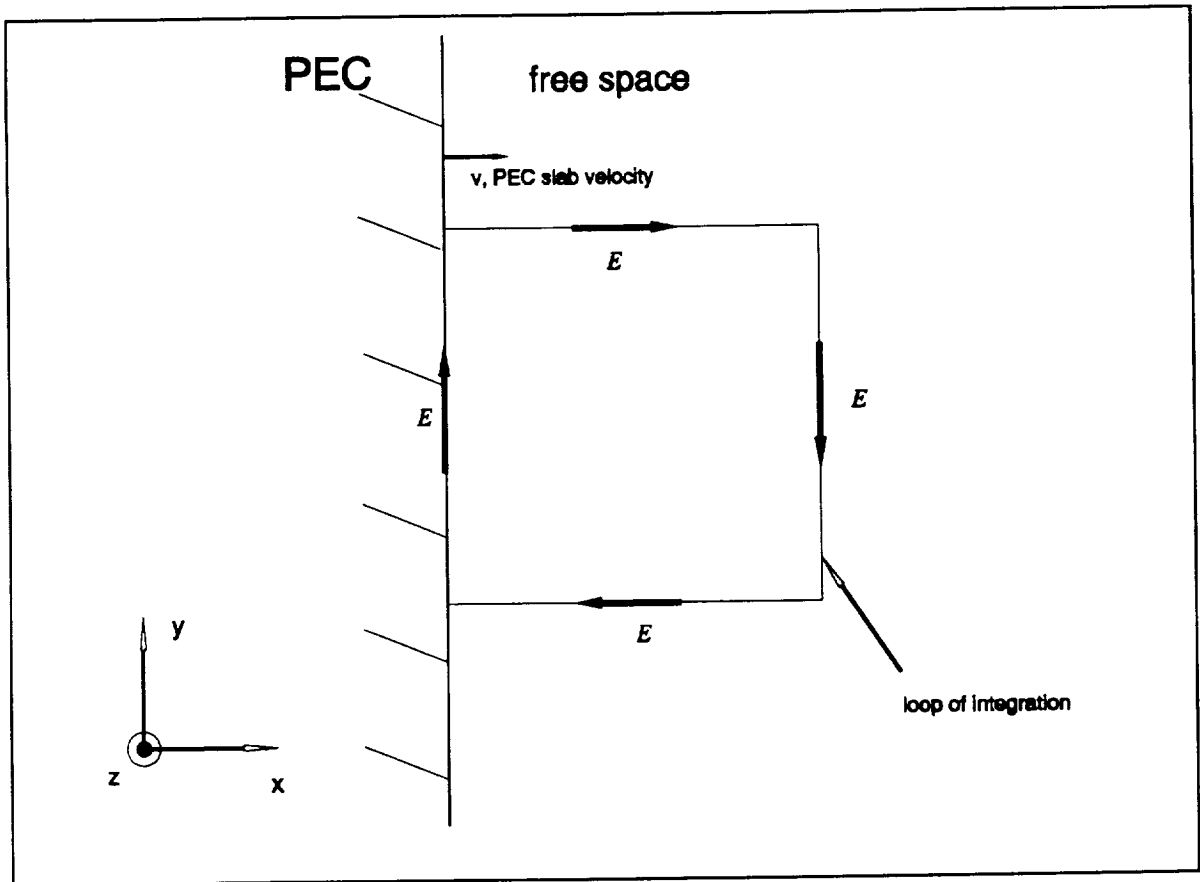
Centerline Slice

# Blade for Zeroth Order Model

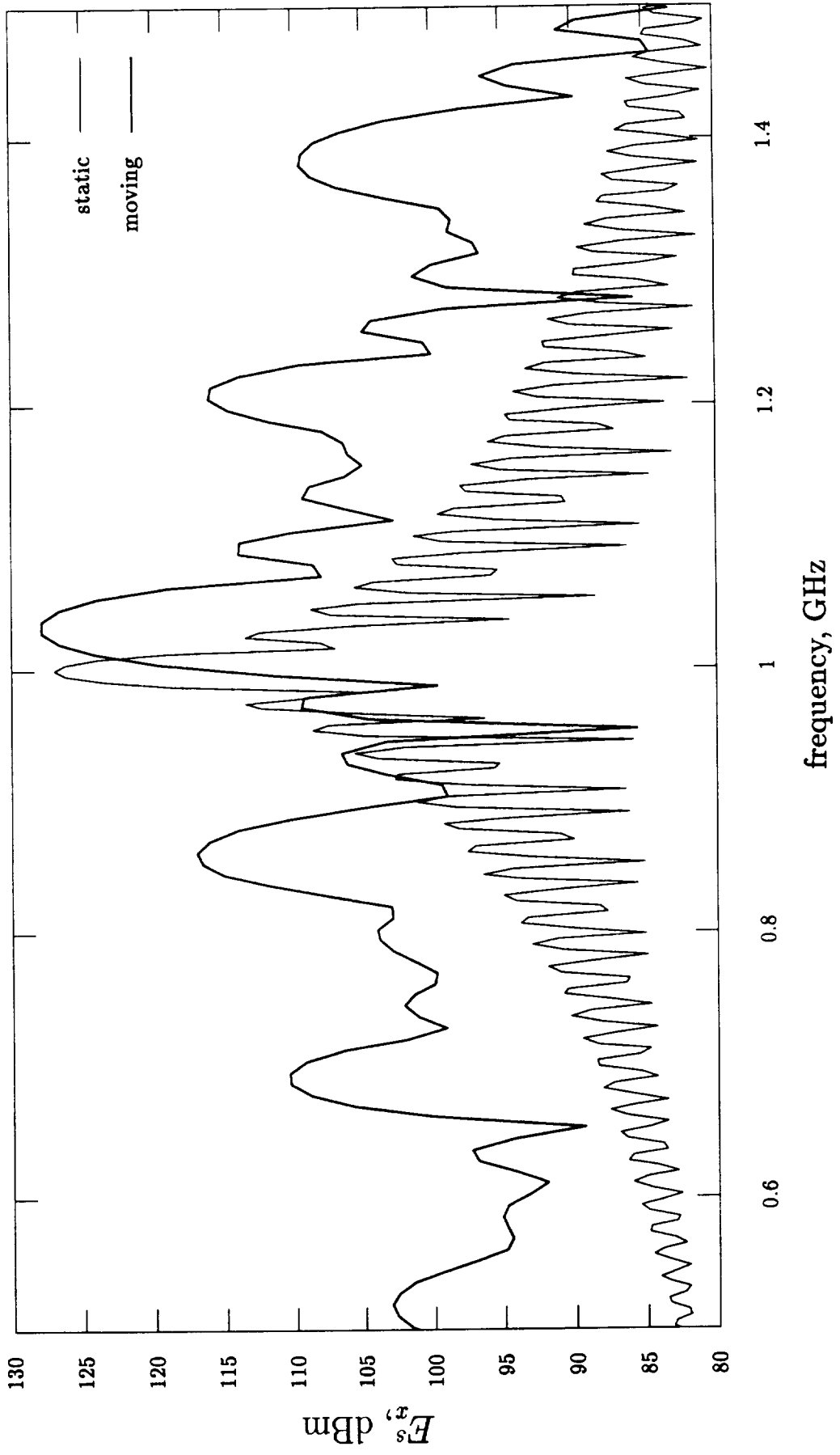


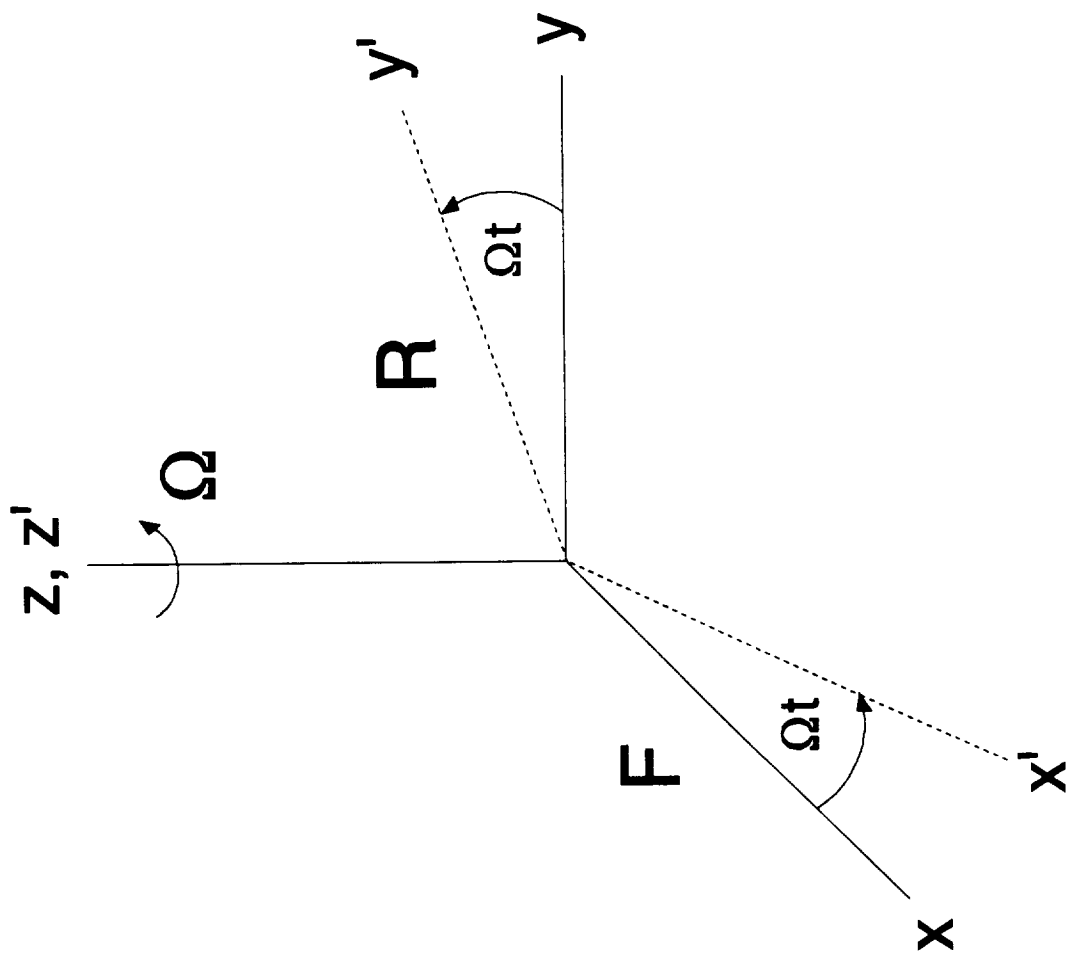
# "Jumping-Cell" Moving Slab

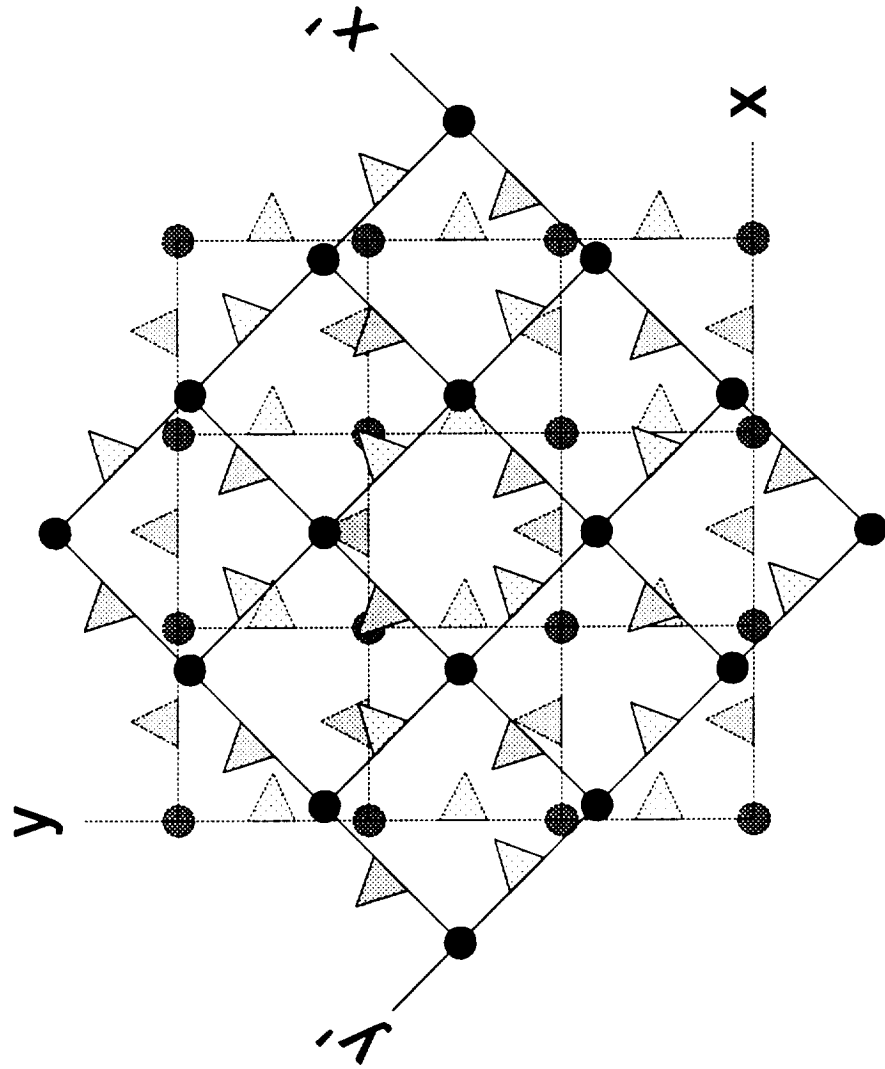




# "Growing-Cell" Moving Slab

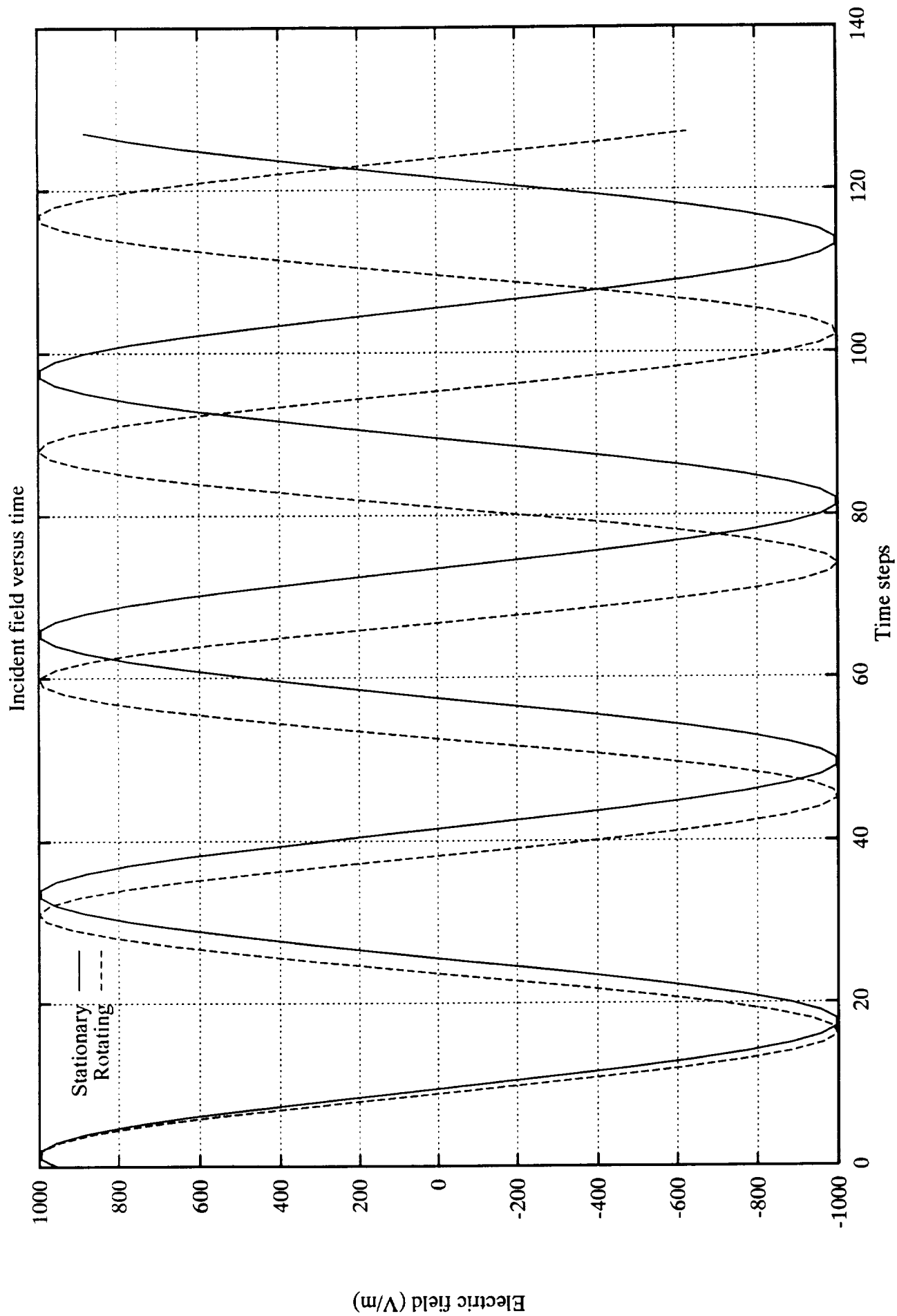






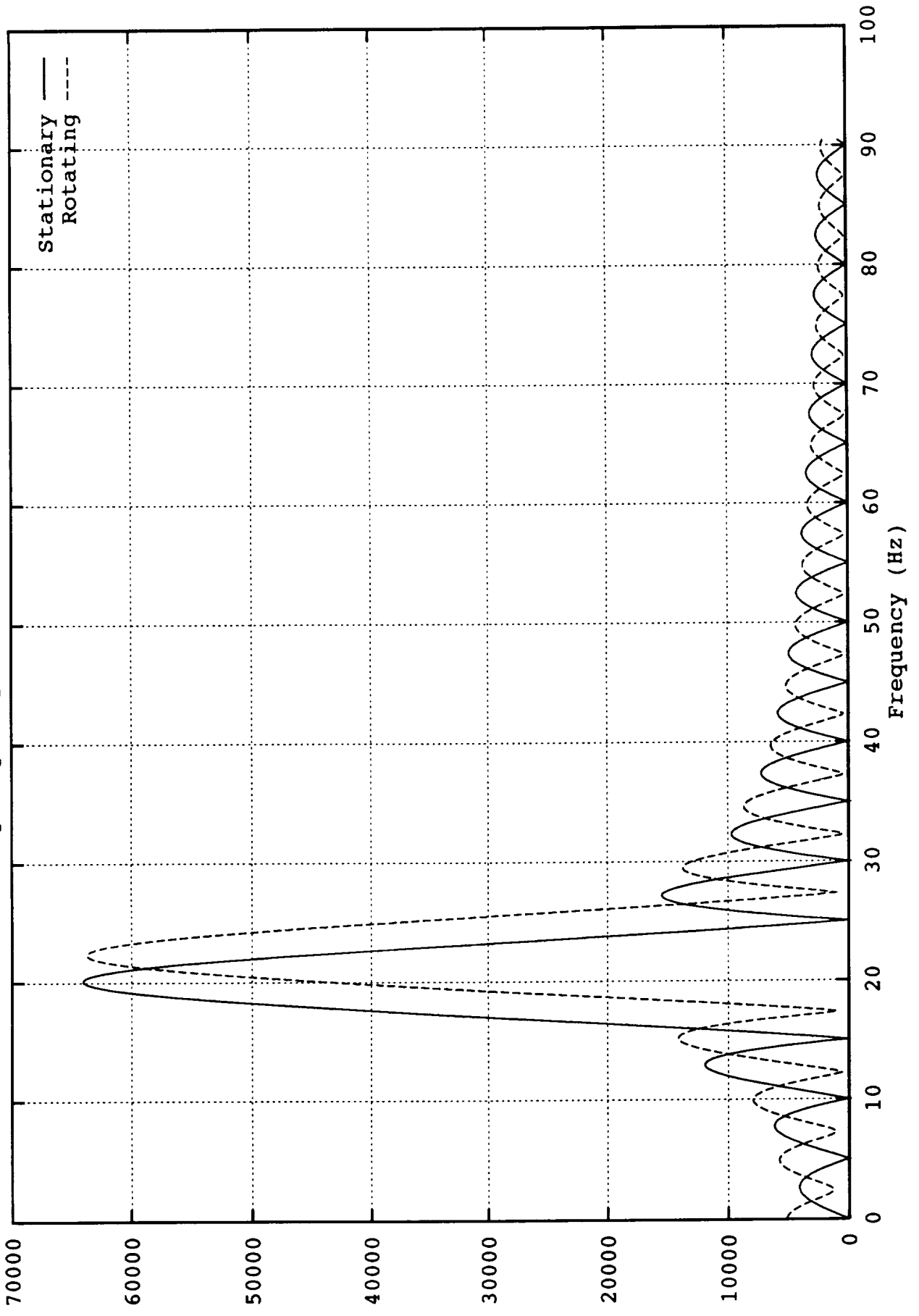
$\bullet = E_z$   
 $\triangle = H_x$   
 $\triangle = H_y$

$\bullet = E'_z$   
 $\triangle = H'_x$   
 $\triangle = H'_y$

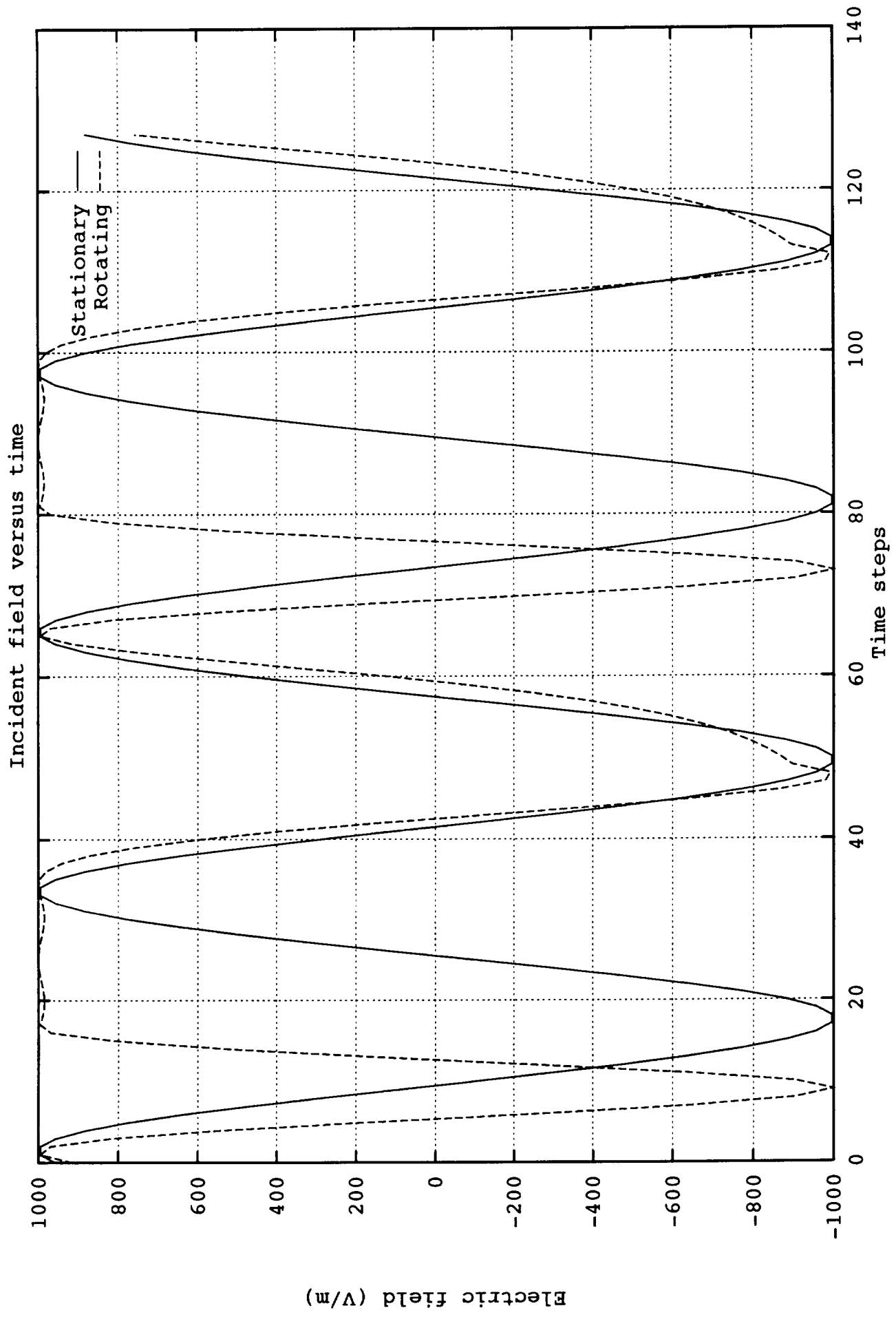




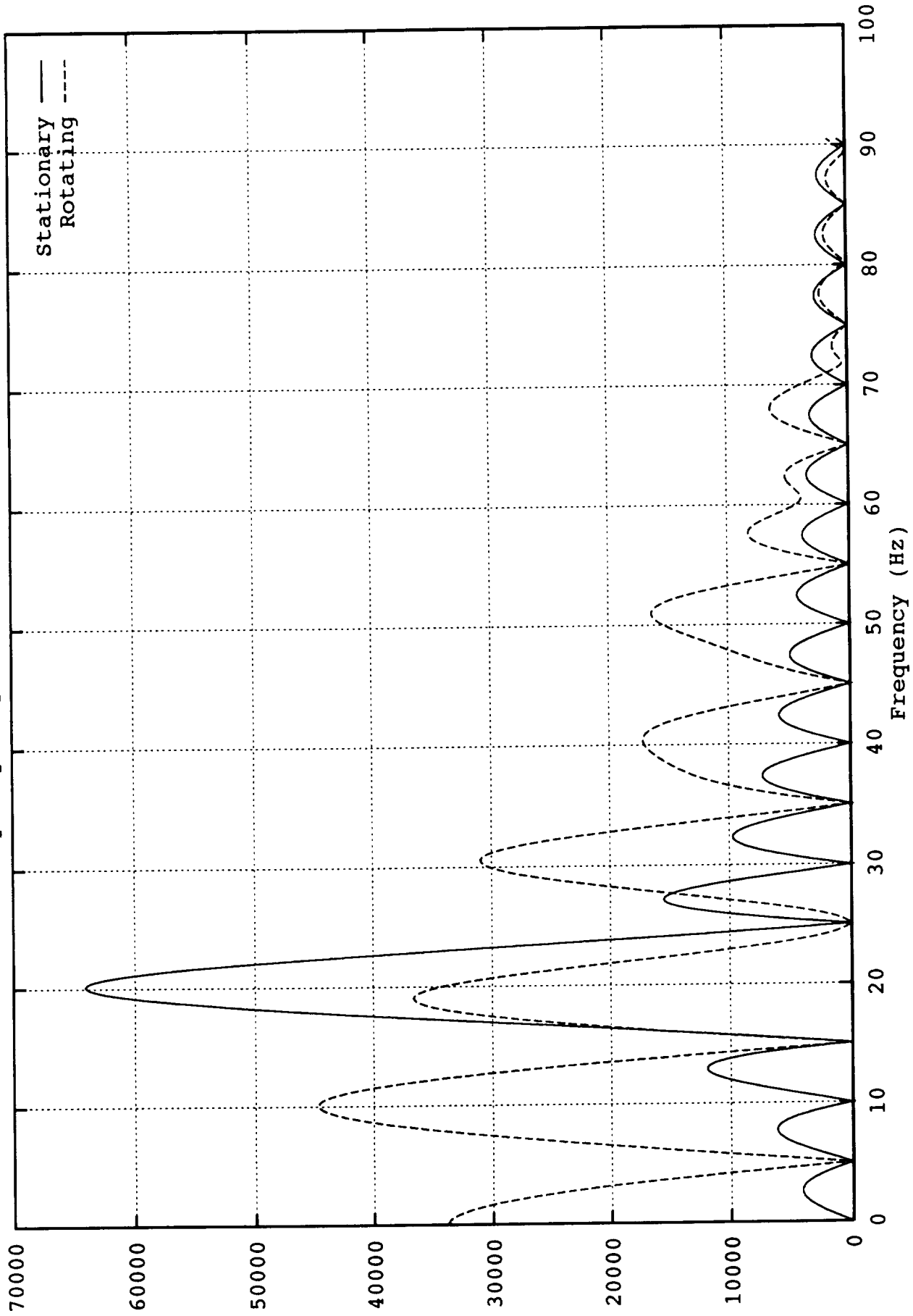
Frequency response of incident field



Magnitude of response



Frequency response of incident field



Magnitude of response